Antiproton-nucleus interaction based on phenomenological, Paris 2009 $\bar{N}N$ and EFT $\bar{N}N$ potentials.

Jaroslava Hrtánková

Nuclear Physics Institute, Řež, Czech Republic

Antiproton-nucleus interactions and related phenomena, 17 - 21 June, ECT* Trento

Motivation

- study of $\bar{p}$ interaction with selected nuclei:

  - behavior of $\bar{p}$ in the nuclear medium
  - $\bar{p}$ absorption in a nucleus
  - testing models of (anti)baryon–baryon interactions as well as models for nuclear structure calculations
  - knowledge of $\bar{p}$–nucleus interaction for future experiments (PANDA@FAIR)

- study of $\bar{p}$-nucleus quasi-bound states $\rightarrow$ possibility of long living $\bar{p}$ in the nuclear medium?

  I.N. Mishustin et al., PRC 71 (2005)

- no experimental evidence of deeply bound $\bar{p}$-nuclear states found so far

Introduction

- study of $\bar{p}$-nucleus interaction and calculations of $\bar{p}$ quasi-bound states in various nuclei
  - within phenomenological RMF approach
    J. Hrtánková, J. Mareš, NPA 945 (2016) 197
  - using the scattering amplitudes derived from the Paris $\bar{N}N$ 2009 potential
    J. Hrtánková, J. Mareš, NPA 969 (2018) 45
- study of $\bar{p}$ optical potential in matter based on the EFT $\bar{N}N$ scattering amplitudes (*L. Dai, J. Haidenbauer, U.-G. Meißner, JHEP 1707 (2017) 078*)

Relativistic Mean-Field approach

system of Dirac nucleons coupled to the exchange mesons and the photon field through an effective Lagrangian.

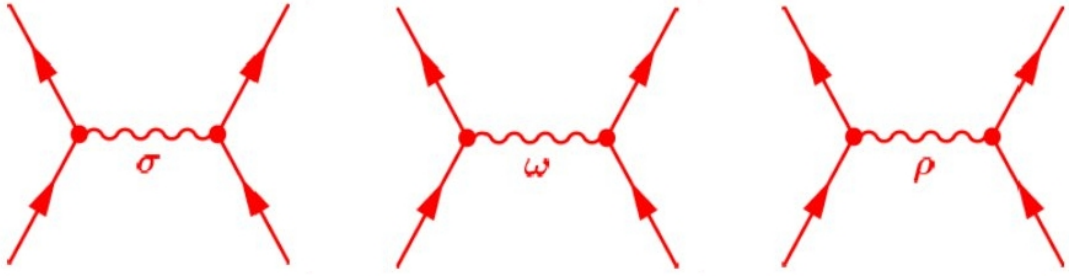

Sigma-meson: attractive scalar field

Omega-meson: short-range repulsive field

Rho-meson: isovector field

- Nucleons treated as Dirac fields interacting via the exchange of boson fields
  - isoscalar-scalar field σ, isoscalar-vector field ω_μ, isovector-vector field $\vec{\rho}_\mu$, and massless vector field A_μ.

Relativistic Mean-Field approach

- Dirac equation for nucleons and antiproton

$$[-i\vec{\alpha}\vec{\nabla} + \beta(m_j + S_j) + V_j]\psi_j^\alpha = \epsilon_j^\alpha \psi_j^\alpha \ , \quad j = N, \bar{p} \ ,$$

$$S = g_{\sigma j}\sigma, \quad V_j = g_{\omega j}\omega_0 + g_{\rho j}\rho_0\tau_3 + e_j\frac{1+\tau_3}{2}A_0 \ ,$$

- Klein-Gordon equations for boson fields

$$\begin{aligned}
(-\triangle + m_\sigma^2 + g_2\sigma + g_3\sigma^2)\sigma &= -g_{\sigma N}\rho_S - g_{\sigma\bar{p}}\rho_{S\bar{p}} \\
(-\triangle + m_\omega^2 + d\omega_0^2)\omega_0 &= g_{\omega N}\rho_V + g_{\omega\bar{p}}\rho_{V\bar{p}} \\
(-\triangle + m_\rho^2)\rho_0 &= g_{\rho N}\rho_I + g_{\rho\bar{p}}\rho_{I\bar{p}} \\
-\triangle A_0 &= e\rho_C + e_{\bar{p}}\rho_{C\bar{p}}.
\end{aligned}$$

- g_{iN}, m_i – RMF models TM1(2), NL-SH and TW9

$\bar{p}$-nucleus interaction

- $NN \to \overline{N}N$ interaction – G-parity transformation $\hat{G} = \hat{C}e^{i\pi I_1}$

$$g_{\sigma\bar{p}} = g_{\sigma N}, \quad g_{\omega\bar{p}} = -g_{\omega N}, \quad g_{\rho\bar{p}} = g_{\rho N}$$

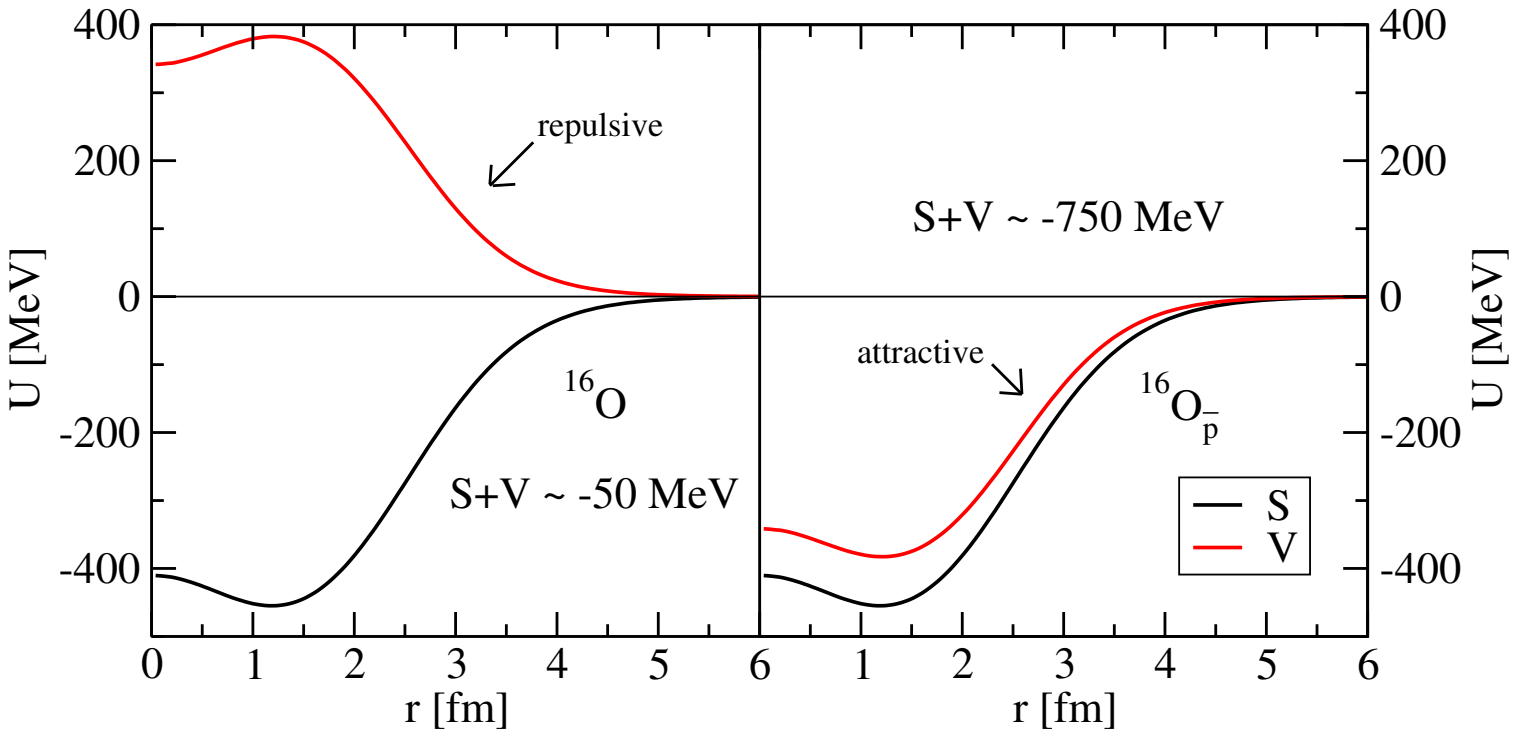

Fig.1: The scalar and vector potential acting on nucleon in ^{16}O (left) and $\bar{p}$ in $^{16}O_{\bar{p}}$ (right), calculated statically in the TM2 model.

$\bar{p}$-nucleus interaction

- G-parity valid for the long and medium range $\bar{N}N$ potential
  $\rightarrow$ 750 MeV deep $\bar{p}$ potential in the nucleus
- Nuclear medium + short range interactions – possible deviations from the G-parity
- Antiprotonic atoms and $\bar{p}$ scattering off nuclei at low energies
  $\rightarrow$ $\mathrm{ReV}_{\bar{p}} \sim 100 - 300$ MeV deep
- Reduced $\bar{p}$ coupling constants

$$g_{\sigma\bar{p}} = \xi\, g_{\sigma N}, \quad g_{\omega\bar{p}} = -\xi\, g_{\omega N}, \quad g_{\rho\bar{p}} = \xi\, g_{\rho N}\ ,$$

where parameter $\xi = 0.2$

$\bar{p}$ absorption

- $\bar{p}$–nucleus potential:

$$\mathrm{Re}\, V_{\bar{p}} = \xi V_{\mathrm{RMF}}$$

$$\mathrm{Im}\, V_{\bar{p}} = \sum_{channel} f_s(\sqrt{s}) B_r \mathrm{Im}\, b_0 \rho$$

$$\xi = 0.2,\ \mathrm{Im}\, b_0 = 1.9\ \mathrm{fm}$$

(*E. Friedman et al., NPA 761 (2005)*)

- longer $\bar{p}$ lifetime due to phase space suppression?

(*I. Mishustin et al., PRC 71 (2005)*)

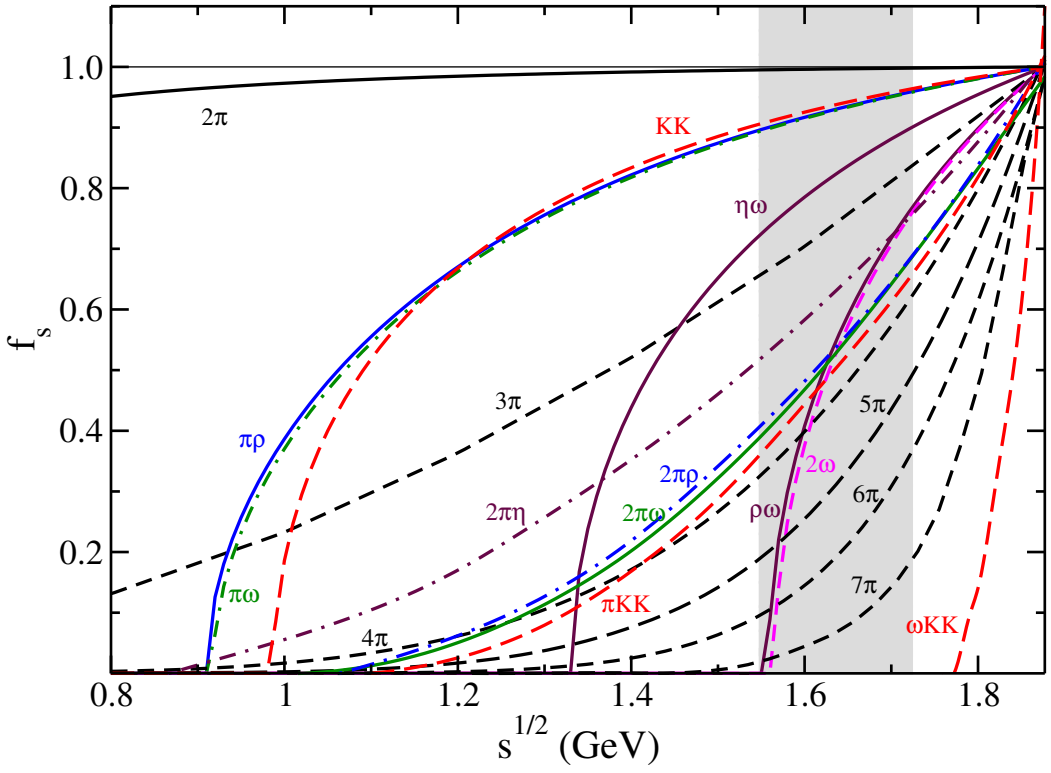

Fig.2: The phase space suppression factor f_s as a function of the center-of-mass energy $\sqrt{s}$.

$\bar{p}$ in the nuclear medium

$\rightarrow$ two-body frame $s_{\rm CMS} = (E_N + E_{\bar{p}})^2 = (m_{\bar{p}} + m_N - B_{\bar{p}} - B_N)^2$

$\rightarrow$ $\bar{p}$ absorption in a nucleus $s_{\rm NUC} = (E_N + E_{\bar{p}})^2 - (\vec{p}_N + \vec{p}_{\bar{p}})^2 \longrightarrow$ $\vec{p}_N + \vec{p}_{\bar{p}} \neq 0$

(A. Cieplý, E. Friedman, A. Gal, D. Gazda, J. Mareš, PLB 702 (2011) 402)

Table 1: Binding energies $B_{\bar{p}}$ and widths $\Gamma_{\bar{p}}$ (in MeV) of the $1s$ $\bar{p}$-nuclear state in ^{16}O, calculated dynamically (Dyn) and statically (Stat) within the TM2 model using the real and complex potentials consistent with $\bar{p}$–atom data.

	Real		Complex		f_s(CMS)		f_s(NUC)	
	Dyn	Stat	Dyn	Stat	Dyn	Stat	Dyn	Stat
$B_{\bar{p}}$	193.7	137.1	175.6	134.6	190.2	136.1	191.5	136.3
$\Gamma_{\bar{p}}$	-	-	552.3	293.3	232.5	165.0	182.3	147.0

Microscopic approach

- complex optical potential $V_{\rm opt}(r)$

$$2E_{\bar{p}}V_{\rm opt}(r) = q(r) + 3\vec{\nabla}\cdot\alpha(r)\vec{\nabla} \ ,$$

with $E_{\bar{p}} = m_{\bar{p}} - B_{\bar{p}}$

- S-wave part is constructed in a '$t\rho$' form

$$q(r) = -4\pi\left[F_0\frac{1}{2}\rho_p(r) + F_1\left(\frac{1}{2}\rho_p(r) + \rho_n(r)\right)\right] \ ,$$

where F_0 and F_1 – isospin 0 and 1 in-medium amplitudes, $\rho_p(r)$ ($\rho_n(r)$) is the proton (neutron) density distribution calculated in the RMF NL-SH model

- $\bar{p}$ binding energies and widths are obtained by solving the Dirac equation

$$[-i\vec{\alpha}\cdot\vec{\nabla} + \beta m_{\bar{p}} + V_{\rm opt}(r) + V_C]\psi_{\bar{p}} = \epsilon_{\bar{p}}\psi_{\bar{p}} \ ,$$

$m_{\bar{p}}$ is the $\bar{p}$ mass, $\epsilon_{\bar{p}} = -B_{\bar{p}} - i\frac{\Gamma_{\bar{p}}}{2}$, $(B > 0)$

Scattering amplitudes

- in-medium amplitudes F_1 and F_0 obtained from free-space S-wave amplitudes using multiple scattering approach (WRW)
  (*T. Wass, M. Rho, W. Weise, NPA 617 (1997) 449*)

$$F_1 = \frac{\frac{\sqrt{s}}{m_N} f^S_{\bar{p}n}(\delta\sqrt{s})}{1 + \frac{1}{4}\xi_k \frac{\sqrt{s}}{m_N} f^S_{\bar{p}n}(\delta\sqrt{s})\rho(r)} \, , F_0 = \frac{\frac{\sqrt{s}}{m_N}[2f^S_{\bar{p}p}(\delta\sqrt{s}) - f^S_{\bar{p}n}(\delta\sqrt{s})]}{1 + \frac{1}{4}\xi_k \frac{\sqrt{s}}{m_N}[2f^S_{\bar{p}p}(\delta\sqrt{s}) - f^S_{\bar{p}n}(\delta\sqrt{s})]\rho(r)} \, ,$$

where $\delta\sqrt{s} = \sqrt{s} - E_{\text{th}}$, $\xi_k = \frac{9\pi}{p_f^2} 4\int_0^\infty \frac{dt}{t} \exp(iqt) j_1^2(t)$ and $q = \frac{1}{p_f}\sqrt{E_{\bar{p}}^2 - m_{\bar{p}}^2}$

- free-space amplitudes $\rightarrow$ 2009 version of the Paris $\bar{N}N$ potential
  (*B. El-Bennich, M. Lacombe, B. Loiseau, S. Wycech, PRC 79 (2009) 054001*)
- Recently used to describe the $\bar{p}$-atom data and low energy $\bar{p}$ scattering off nuclei
  (*E. Friedman, A. Gal, B. Loiseau, S. Wycech, NPA 934 (2015) 101*)

In-medium Paris S-wave amplitudes

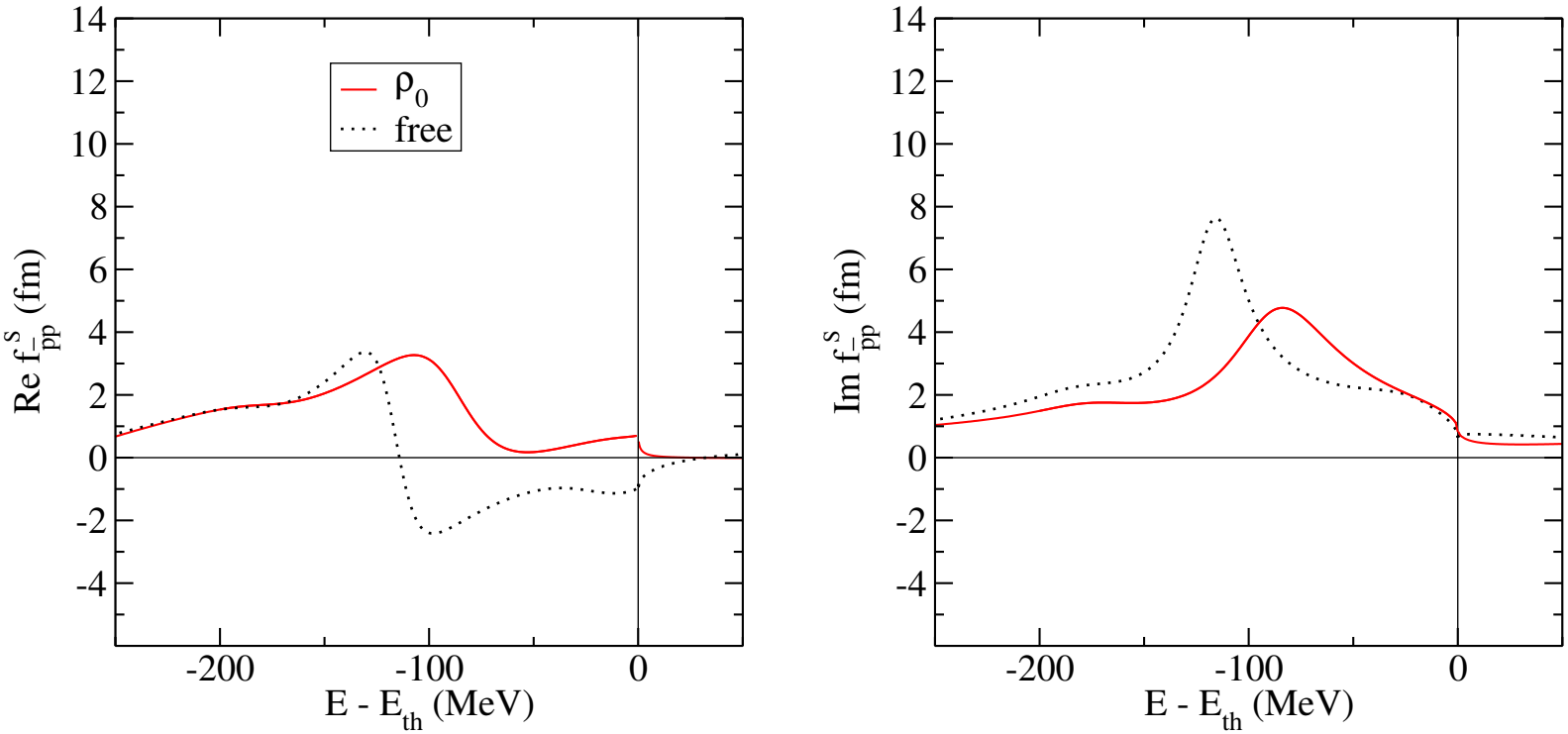

Fig.3: Energy dependence of the Paris 09 $\bar{p}p$ c.m. S-wave amplitudes: Pauli blocked amplitude for $\rho_0 = 0.17$ fm^{-3} (solid lines) compared with free-space amplitude (dotted lines).

In-medium Paris S-wave amplitudes

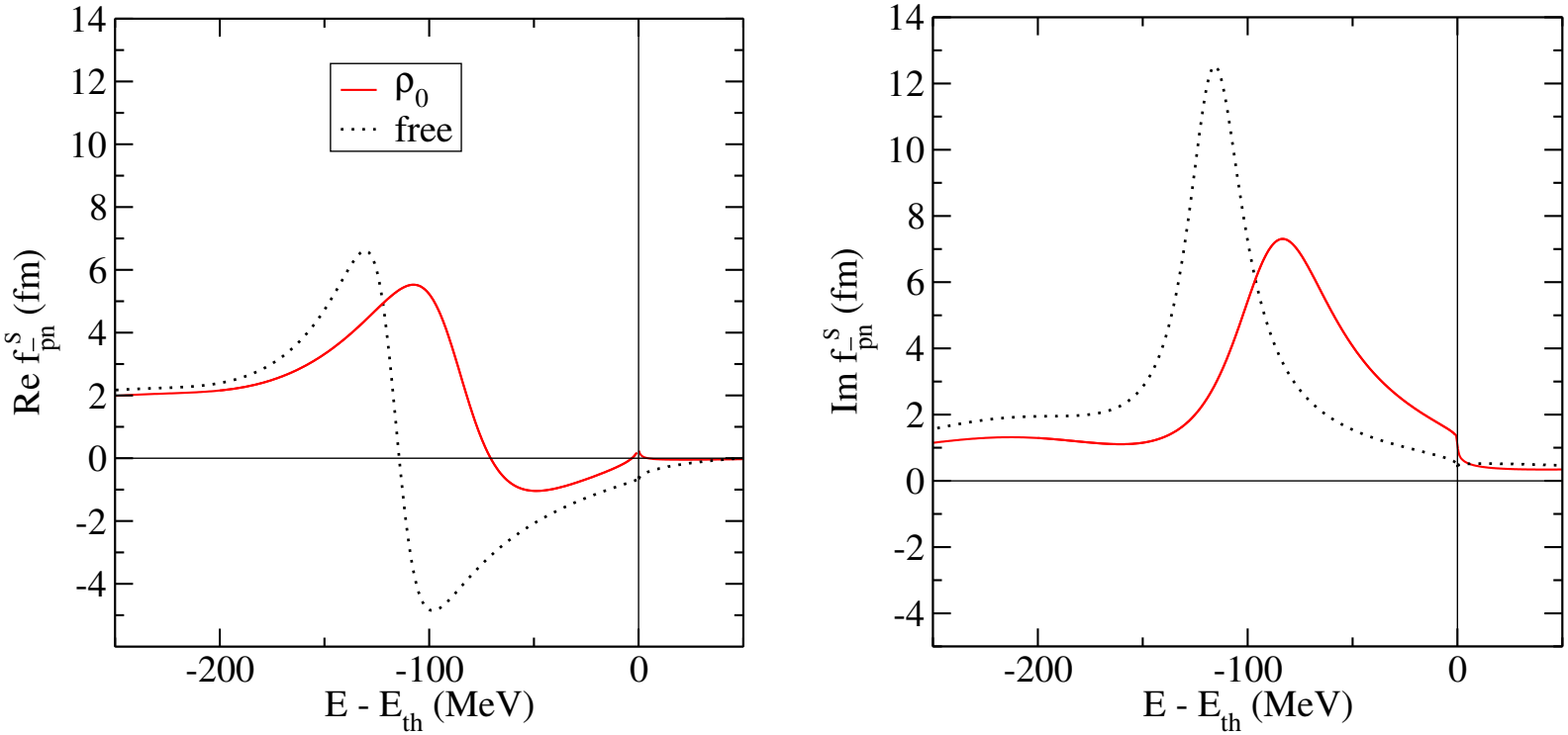

Fig.4: Energy dependence of the Paris 09 $\bar{p}n$ c.m. S-wave amplitudes: Pauli blocked amplitude for $\rho_0 = 0.17$ fm^{-3} (solid lines) compared with free-space amplitude (dotted lines).

Paris P-wave interaction

- The P-wave potential

$$2E_{\bar{p}}V_{\mathrm{opt}}(r) = q(r) + 3\vec{\nabla}\cdot\alpha(r)\vec{\nabla} \ ,$$

where

$$\alpha(r) = 4\pi\frac{m_N}{\sqrt{s}}\left(f^P_{p\bar{p}}(\delta\sqrt{s})\rho_p(r) + f^P_{n\bar{p}}(\delta\sqrt{s})\rho_n(r)\right) \ .$$

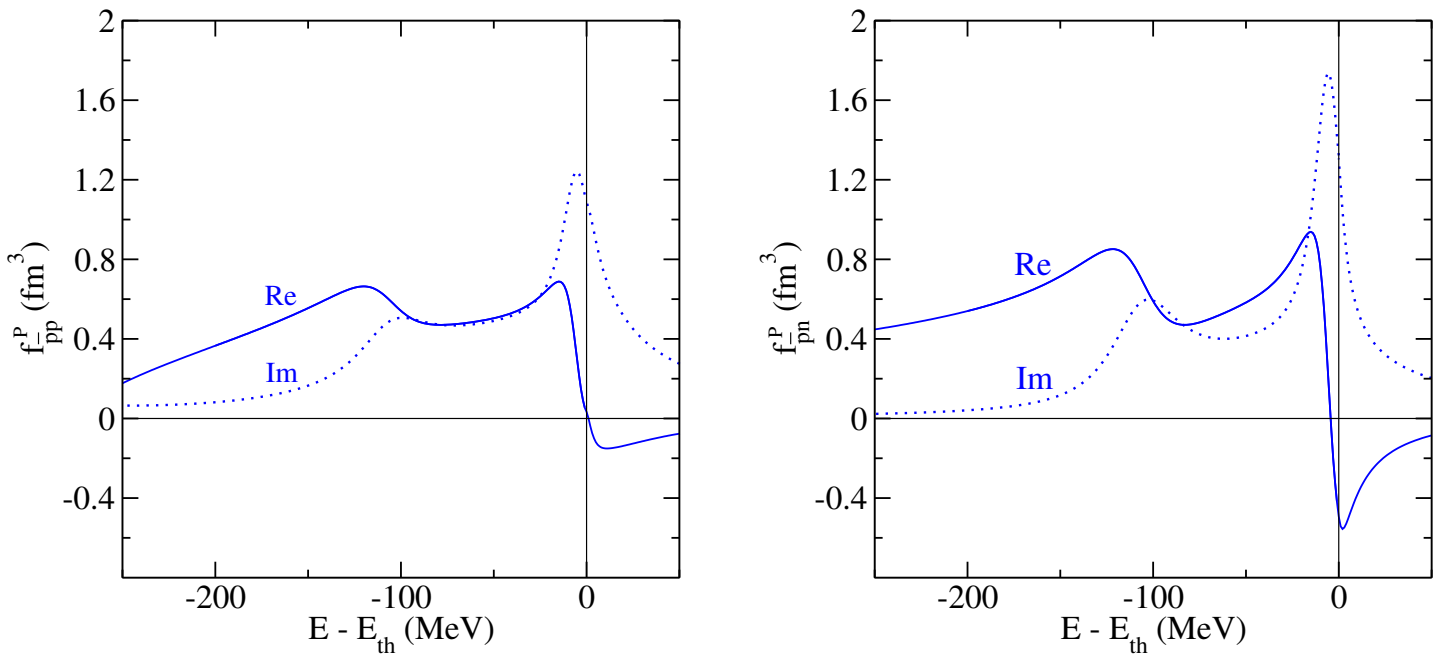

Fig.5: Energy dependence of the Paris 09 $\bar{p}p$ (left) and $\bar{p}n$ (right) c.m. free-space P-wave amplitudes.

P-wave interaction

- $S + P$-wave Paris potential does not fit the $\bar{p}$ atom data
- S-wave Paris potential + phenomenological P-wave
  $f^P_{\bar{p}N} = 2.9 + \mathrm{i}1.8$ fm^3 yields satisfactory agreement with the atom data
  (*E. Friedman, A. Gal, B. Loiseau, S. Wycech, NPA 934 (2015) 101)*

Energy dependence

- $\bar{p}N$ Paris amplitudes — functions of energy shift $\delta\sqrt{s} = \sqrt{s} - E_{th}$ where $s = (E_N + E_{\bar{p}})^2 - (\vec{p}_N + \vec{p}_{\bar{p}})^2$

$$\sqrt{s} = E_{th}\left(1 - \frac{2(B_{\bar{p}} + B_{Nav})}{E_{th}} + \frac{(B_{\bar{p}} + B_{Nav})^2}{E_{th}^2} - \frac{1}{E_{th}}T_{\bar{p}} - \frac{1}{E_{th}}T_{Nav}\right)^{1/2},$$

where $B_{Nav} = 8.5$ MeV, $T_{\bar{p}(Nav)}$ is $\bar{p}$ (nucleon) average kinetic energy and $E_{th} = m_N + m_{\bar{p}}$

- self-consistent scheme adopted in calculations

Energy dependence of the S-wave $\bar{p}$ potential

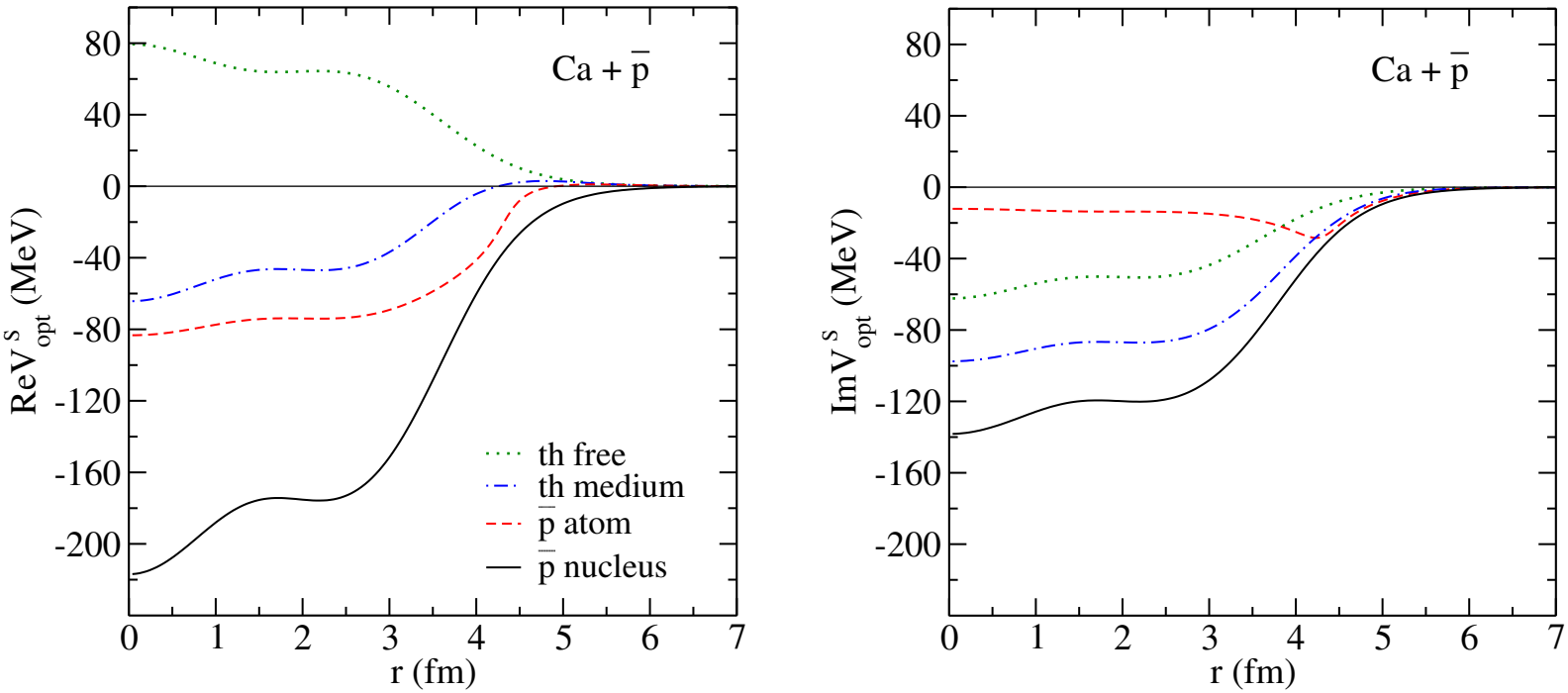

Fig.6: The potential felt by $\bar{p}$ at threshold ('th medium'), in the $\bar{p}$ atom and $\bar{p}$ nucleus, calculated for ^{40}Ca+$\bar{p}$ with in-medium Paris S-wave amplitudes and static RMF densities. The $\bar{p}$ potential calculated using free-space amplitudes at threshold is shown for comparison ('th free').

1s $\bar{p}$ binding energies and widths

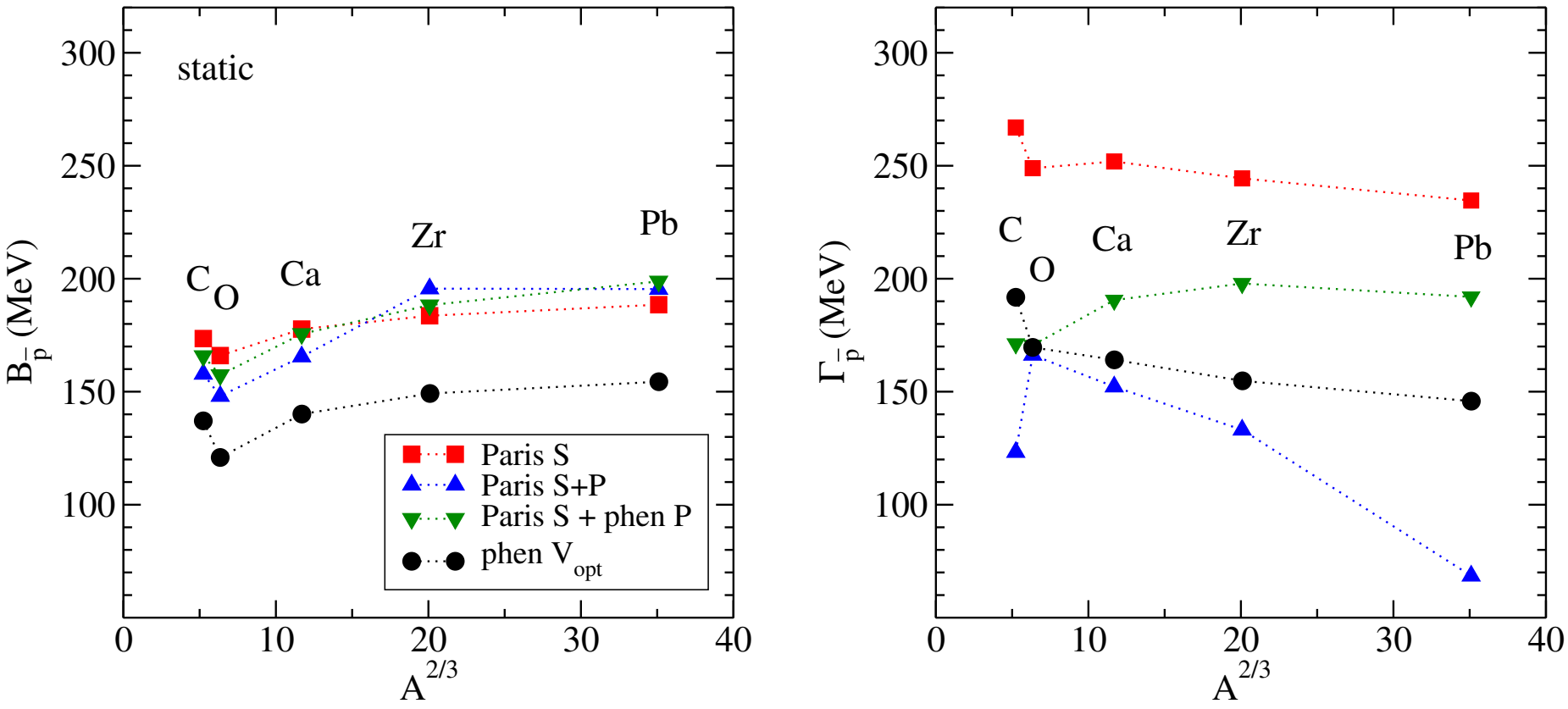

Fig.7: 1s $\bar{p}$ binding energies (left panel) and widths (right panel) in various nuclei, calculated statically using S-wave Paris potential, including phenomenological P-wave potential, Paris P-wave potential and phenomenological RMF potential.

1s $\bar{p}$ binding energies and widths

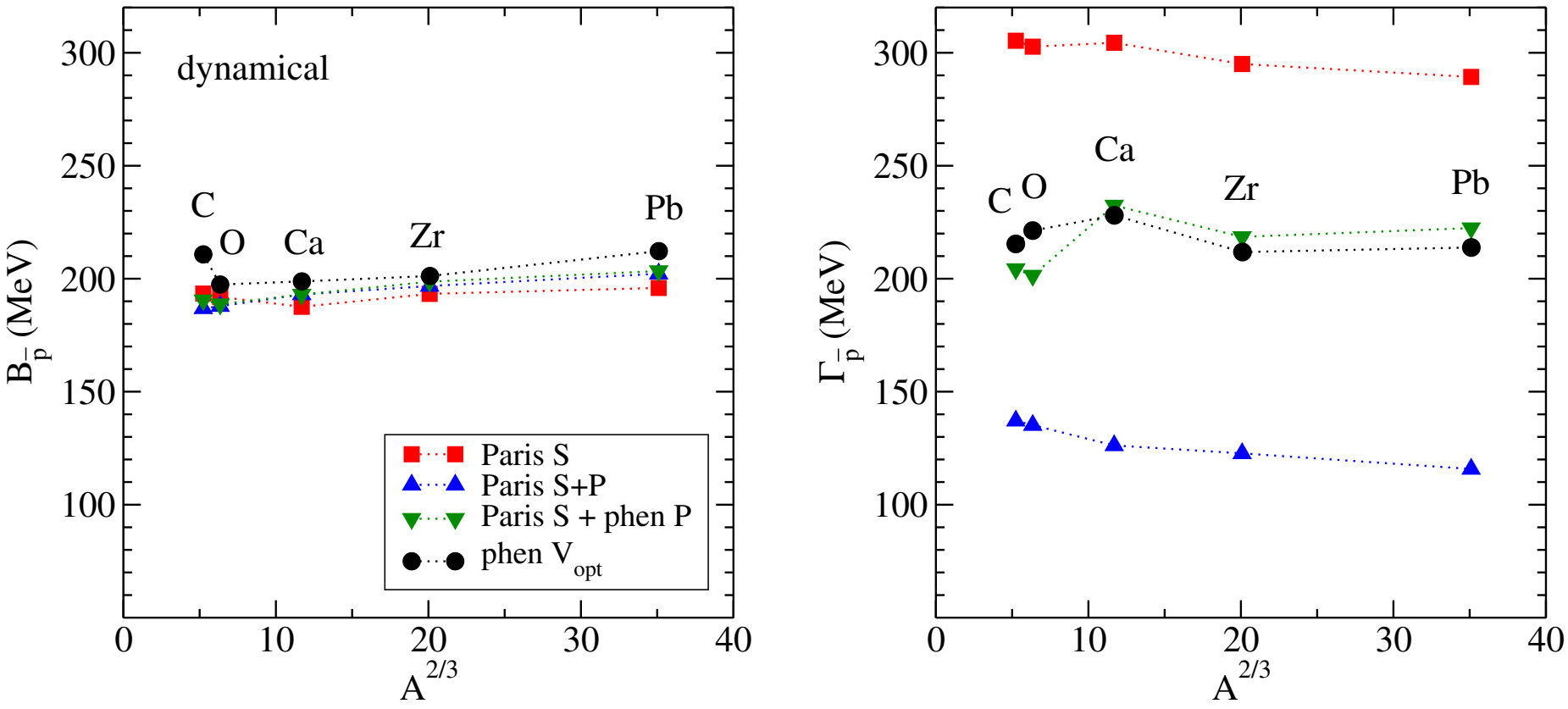

Fig.8: Binding energies (left panel) and widths (right panel) of 1s $\bar{p}$-nuclear states in selected nuclei, calculated dynamically using the Paris $\bar{N}N$ S-wave potential, Paris S-wave + phen. P-wave and phenomenological RMF potential.

$\bar{p}$ binding energies and widths – excited states

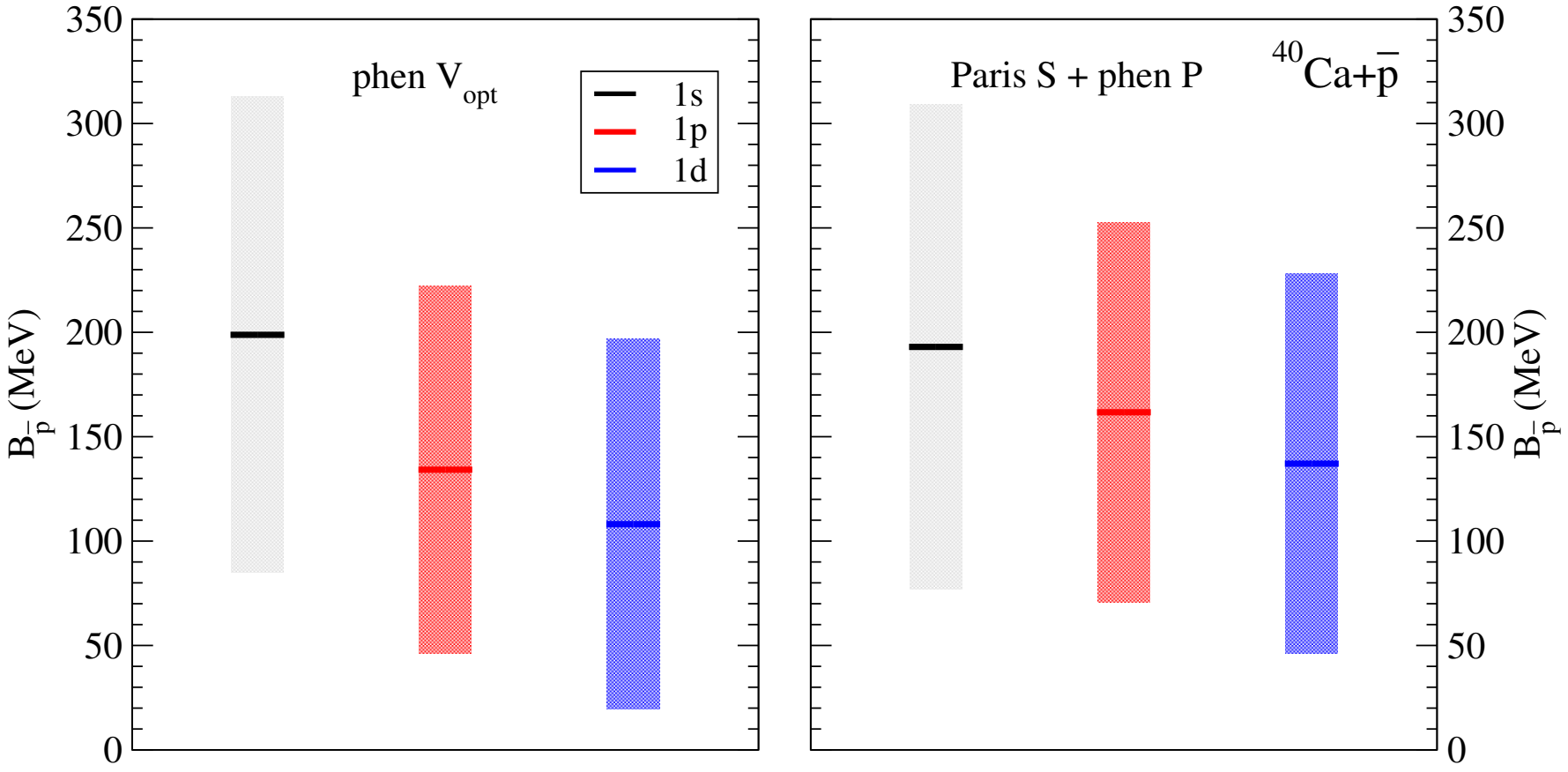

Fig.9:1s, 1p and 1d binding energies (lines) and widths (boxes) of $\bar{p}$ in ^{40}Ca calculated dynamically within the phenomenological RMF $\bar{p}$ optical potential and Paris S-wave + phen. P-wave potential.

Conclusions: calculations of $\bar{p}$ quasi-bound states in nuclei

- phenomenological RMF potential:
  - large polarization effects of the nuclear core due to $\bar{p}$ confirmed
  - $\bar{p}$ widths are suppressed due to the phase space reduction, but still remain large for potentials consistent with $\bar{p}$–atom data
- 2009 version of the Paris $\bar{N}N$ potential:
  - $\bar{p}$ potential is strongly energy dependent
  - P-wave interaction slightly affects the $\bar{p}$ binding energies and decrease noticeably the $\bar{p}$ widths
  - Paris $S + P$-wave potential yields too small $\bar{p}$ widths (also fails to reproduce $\bar{p}$ atom data)
  - Paris S-wave + phenomenological P-wave potential yield comparable $\bar{p}$ binding energies (~ 200 MeV) and widths ($\sim 200 - 230$ MeV) as the phenomenological approach within the RMF model.

Chiral $\bar{N}N$ interaction model

- recently developed chiral $\bar{N}N$ interaction model (N2LO and N3LO)
  (*L. Dai, J. Haidenbauer, U.-G. Meißner*, JHEP 1707 (2017) 078)
- S-wave scattering amplitudes below $\bar{N}N$ threshold:
  - off-shell t-matrix $T(p, p', E)$ where $E = 2\sqrt{m_N^2 + k^2}$
  - two choices for off-shell momenta $\rightarrow p = 0,\ p' = |k|$ ('0k')
    $\rightarrow p = p' = |k|$ ('kk')
- $\bar{p}p$ and $\bar{p}n$ amplitudes constructed as angular-momentum averages over fixed-T amplitudes (same as Paris amplitudes)

$$f_L^T = \frac{\sum_{SJ}(2J+1) f_{LS}^{TJ}}{\sum_{SJ}(2J+1)}$$

- study of $\bar{p}$ optical potential based on chiral $\bar{N}N$ amplitudes in matter

Chiral S-wave scattering amplitudes

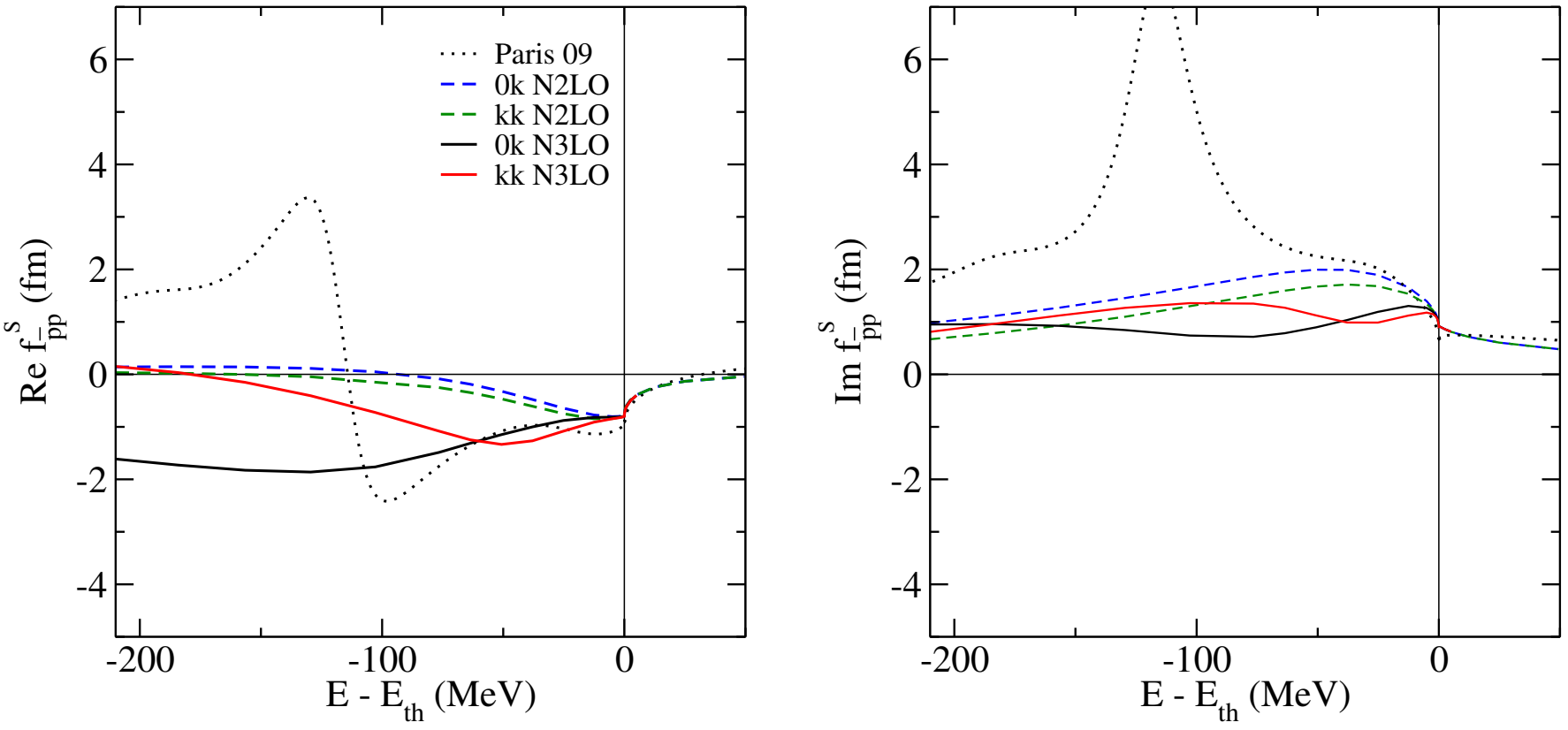

Fig.10: Energy dependence of the chiral N2LO (dashed) and N3LO (solid) $\bar{p}p$ free-space c.m. S-wave amplitudes compared with the Paris $\bar{p}p$ scattering amplitudes.

Chiral S-wave scattering amplitudes

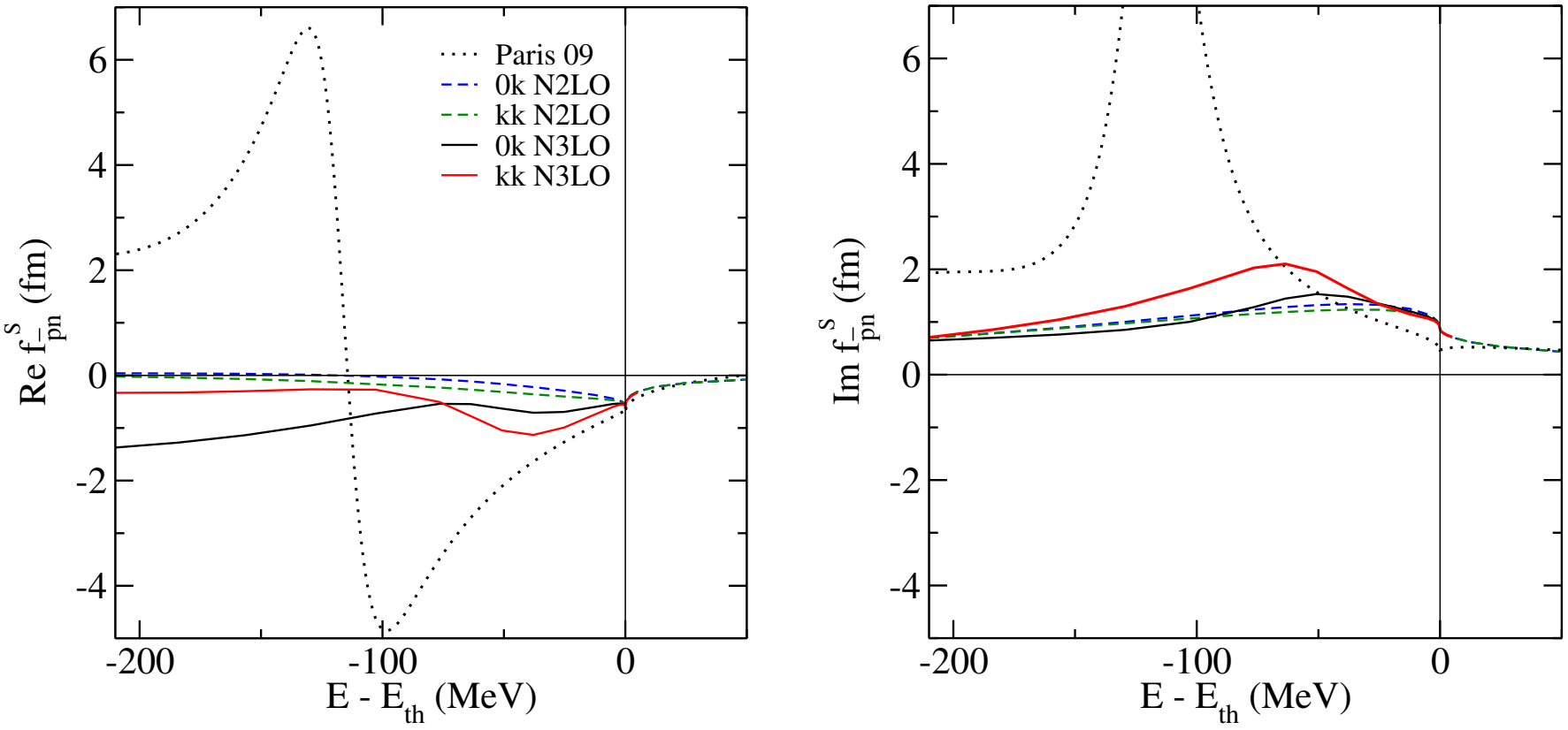

Fig.11: Energy dependence of the chiral N2LO (dashed) and N3LO (solid) $\bar{p}n$ free-space c.m. S-wave amplitudes compared with the Paris $\bar{p}n$ scattering amplitudes.

$\bar{p}$ optical potential in nuclear matter

$\rightarrow$ $\bar{p}$ optical potential as a function of nuclear matter density

$$2E_{\bar{p}}V_{\rm opt}(\rho) = -4\pi\left(\frac{1}{2}F_0\frac{\rho}{2} + F_1\left(\frac{1}{2}\frac{\rho}{2} + \frac{\rho}{2}\right)\right) \ ,$$

ρ - nuclear matter density, $E_{\bar{p}} = m_N - B_{\bar{p}}\frac{\rho}{\rho_0}$, F_1 and F_0 are isospin 1 and 0 in-medium amplitudes

$$F_1 = \frac{f^{\rm S}_{\bar{p}n}(\delta\sqrt{s})}{1+\frac{1}{4}\xi_k f^{\rm S}_{\bar{p}n}(\delta\sqrt{s})\rho} \ , \quad F_0 = \frac{[2f^{\rm S}_{\bar{p}p}(\delta\sqrt{s}) - f^{\rm S}_{\bar{p}n}(\delta\sqrt{s})]}{1+\frac{1}{4}\xi_k[2f^{\rm S}_{\bar{p}p}(\delta\sqrt{s}) - f^{\rm S}_{\bar{p}n}(\delta\sqrt{s})]\rho} \ .$$

- energy shift $\delta\sqrt{s} = \sqrt{s} - E_{\rm th}$ with $\sqrt{s} = \sqrt{(E_{\bar{p}} + E_F)^2 - \frac{3}{5}k_F^2}$

  $E_F = \sqrt{m_N^2 + \frac{3}{5}k_F^2} + V_N\frac{\rho}{\rho_0}$, k_F - Fermi momentum, $V_N = -50$ MeV - potential felt by nucleon in matter at saturation density $\rho_0 = 0.169$ fm^{-3}

In-medium amplitudes

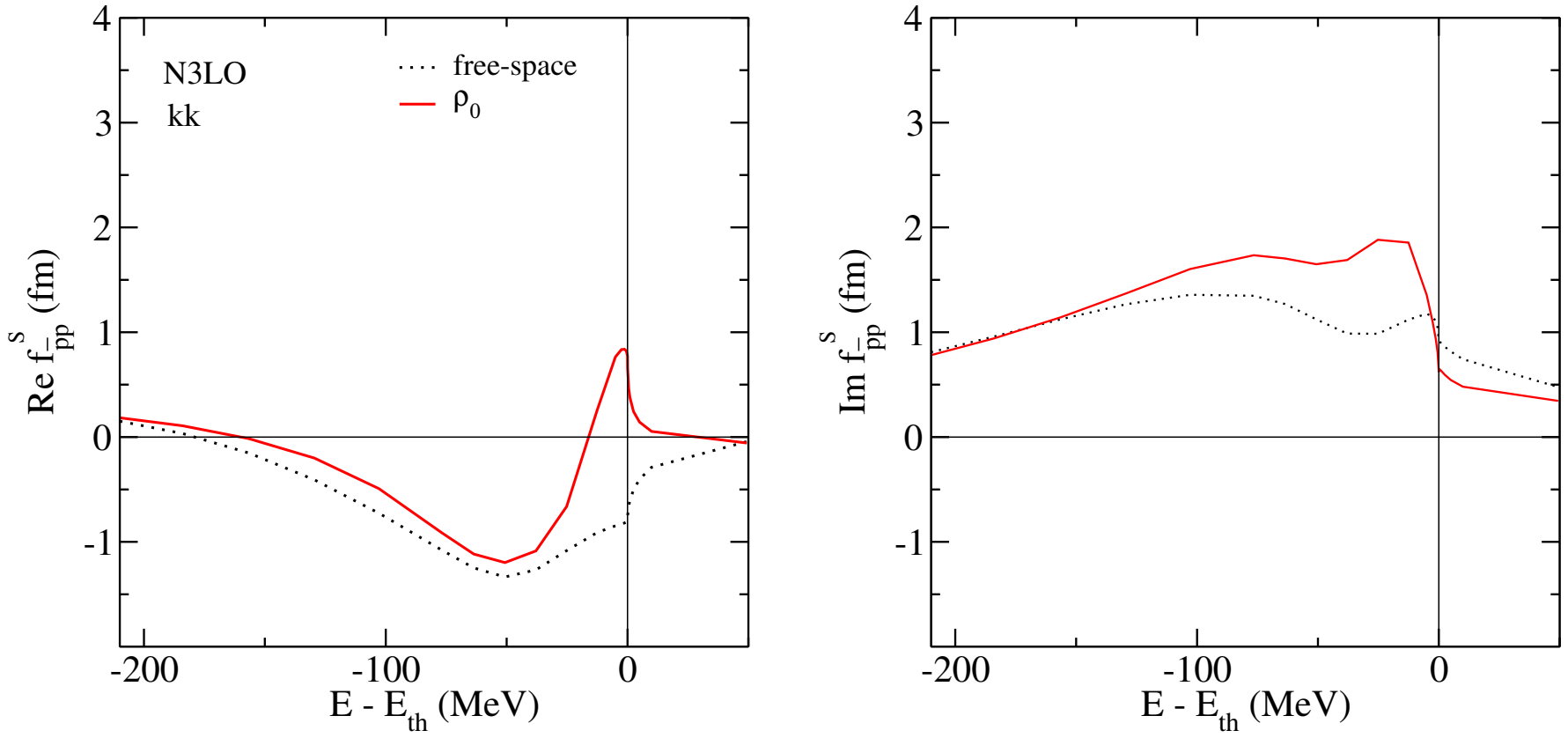

Fig.12: Comparison of free-space $\bar{p}p$ N3LO chiral amplitude (dotted) with medium modified amplitude at ρ_0.

In-medium amplitudes

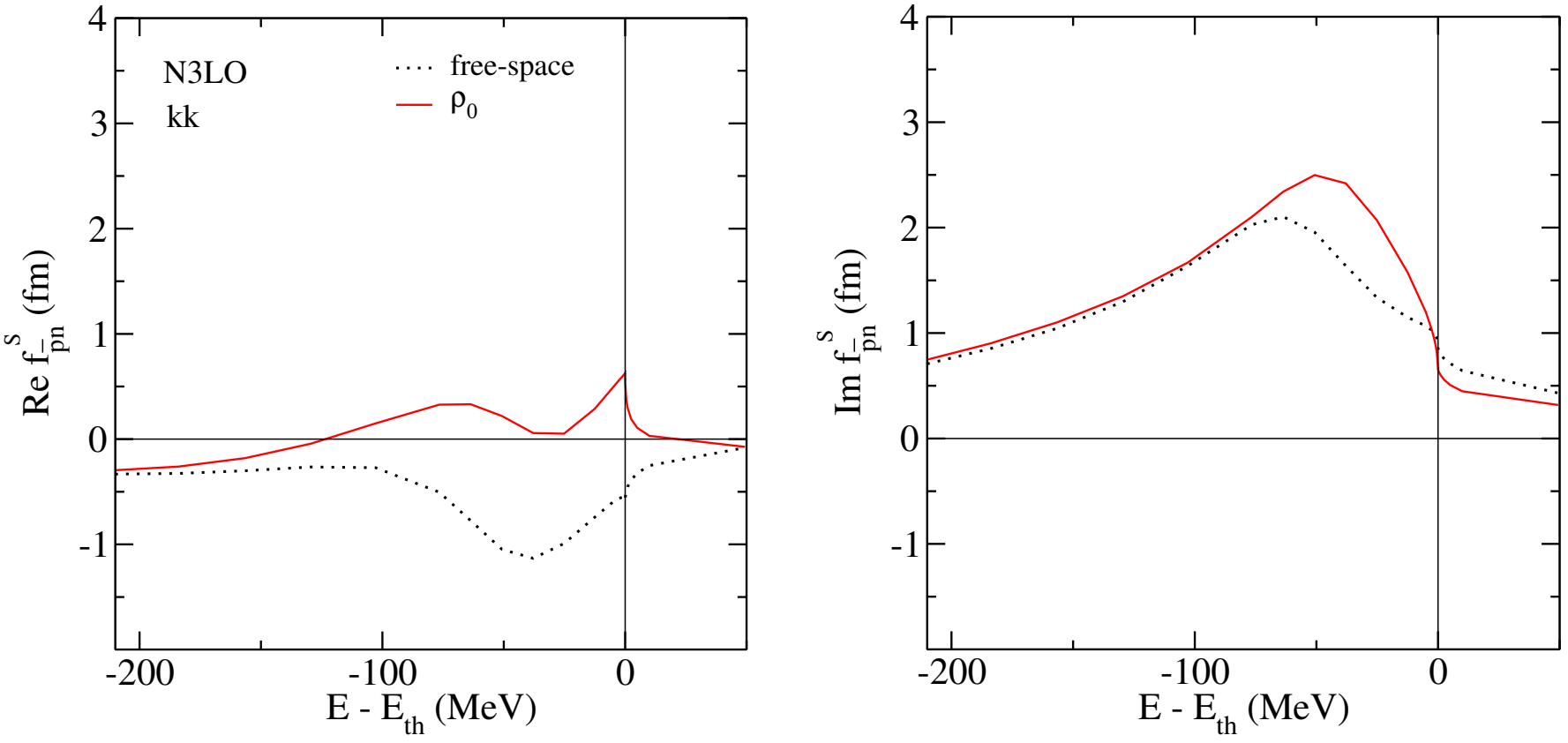

Fig.13: Comparison of free-space $\bar{p}n$ N3LO chiral amplitude (dotted) with medium modified amplitude at ρ_0.

Energies probed below threshold

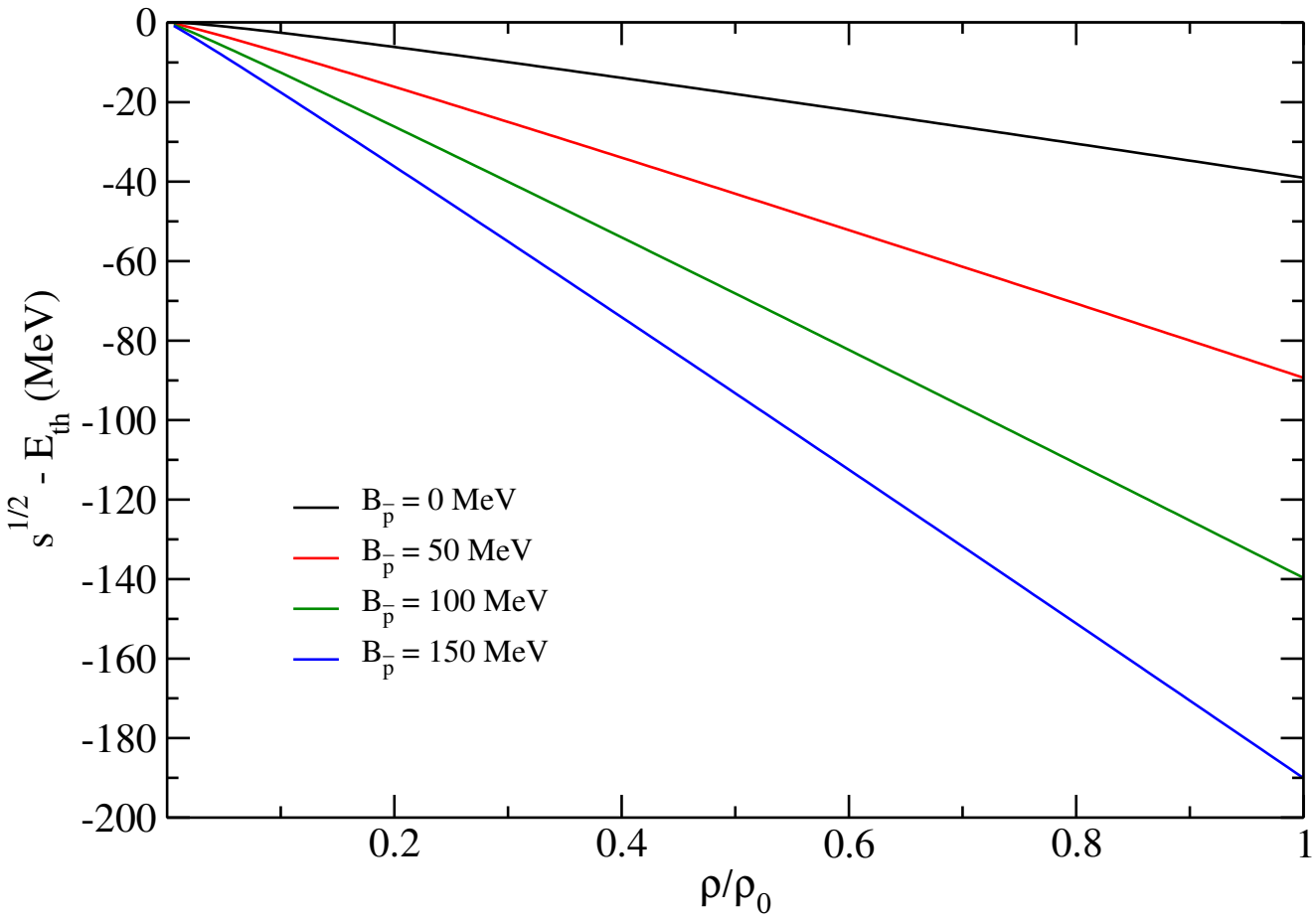

Fig.14: Energies probed below $\bar{N}N$ threshold as a function of relative density for different values of $B_{\bar{p}}$.

N2LO vs. N3LO potentials

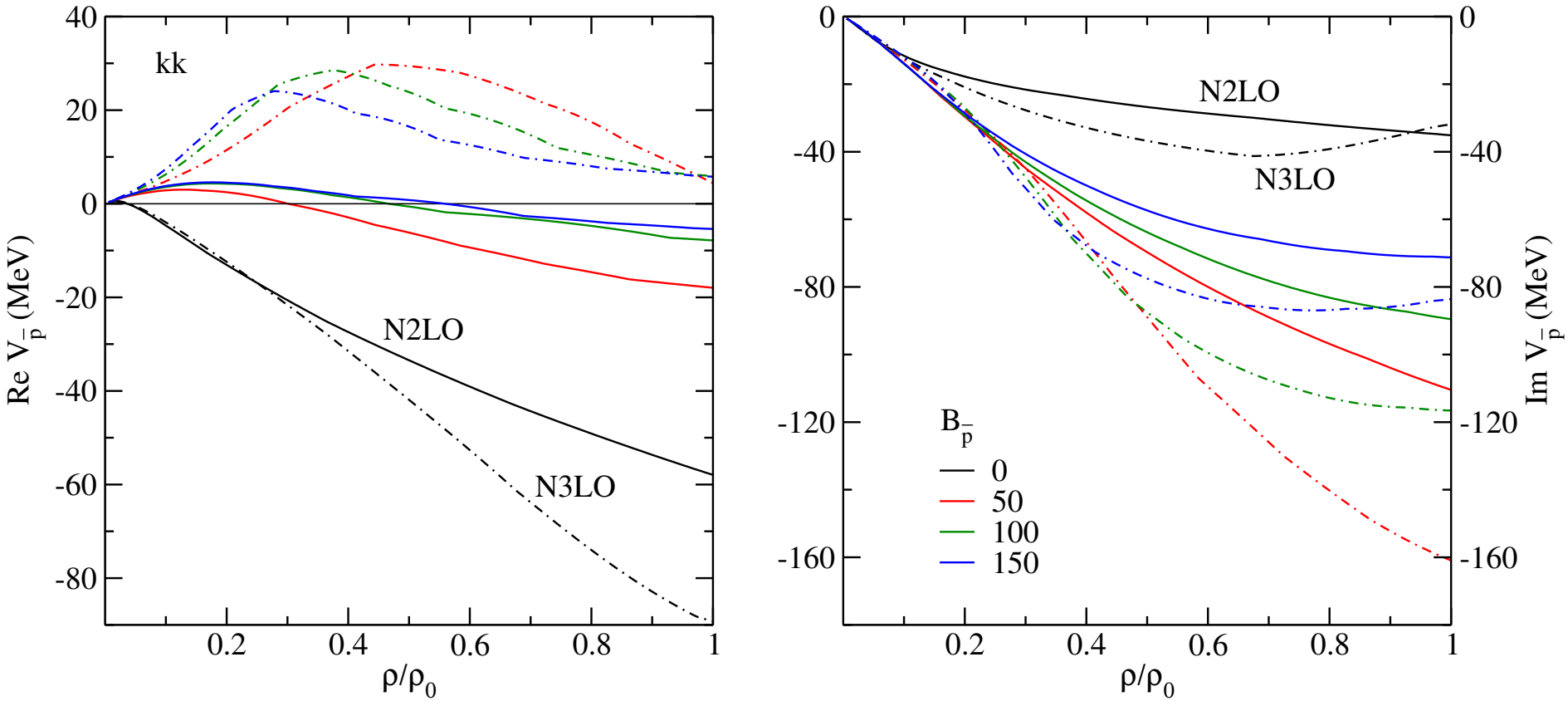

Fig.15: Real (left) and imaginary (right) $\bar{p}$ potentials in nuclear matter, calculated using the on-shell N2LO (solid) and N3LO (dashed-dot) chiral amplitudes for different values of $B_{\bar{p}}$.

N3LO vs. Paris 09 potential

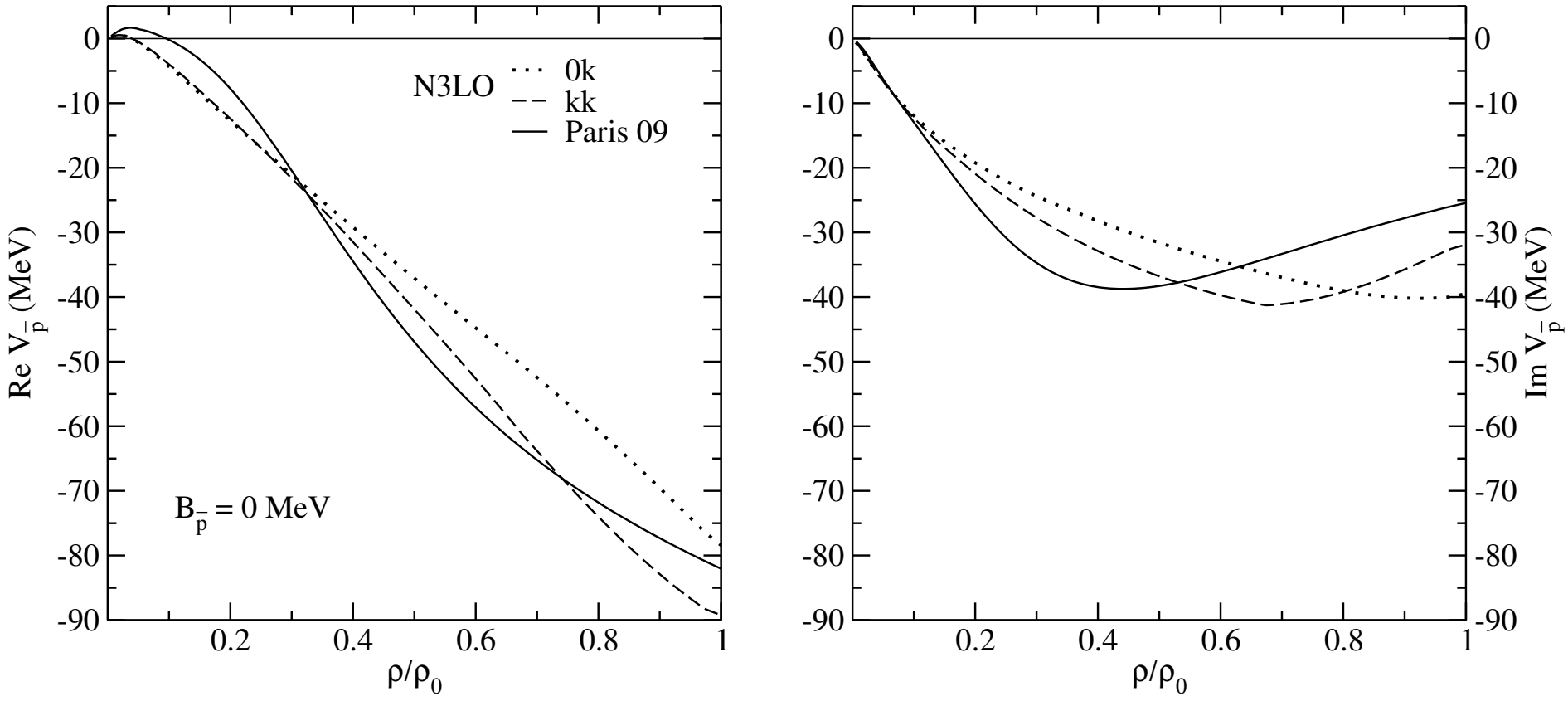

Fig.16: Real (left) and imaginary (right) $\bar{p}$ potentials in nuclear matter, calculated using the chiral N3LO and Paris 09 amplitudes for $B_{\bar{p}} = 0$ MeV.

N3LO vs. Paris 09 potential

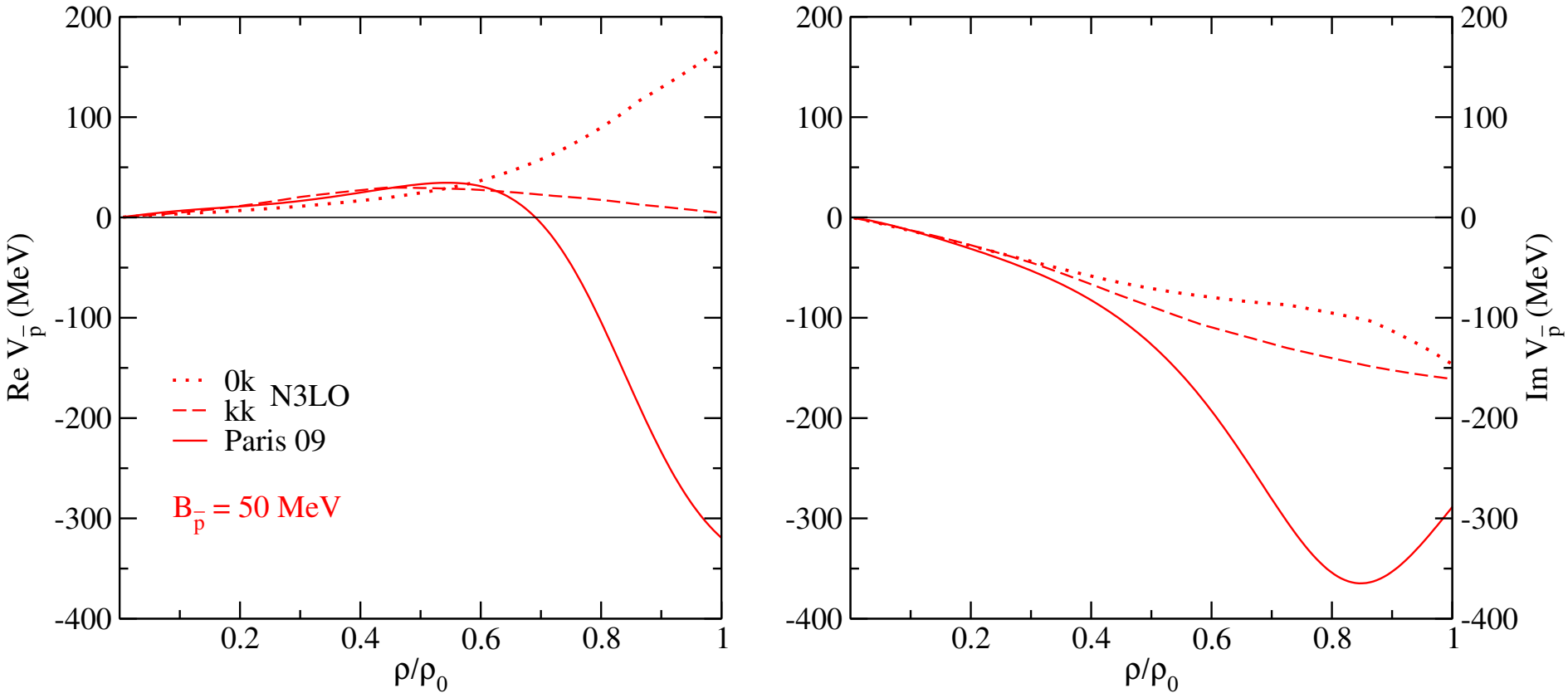

Fig.17: Real (left) and imaginary (right) $\bar{p}$ potentials in nuclear matter, calculated using the chiral N3LO and Paris 09 amplitudes for $B_{\bar{p}} = 50$ MeV.

N3LO vs. Paris 09 potential

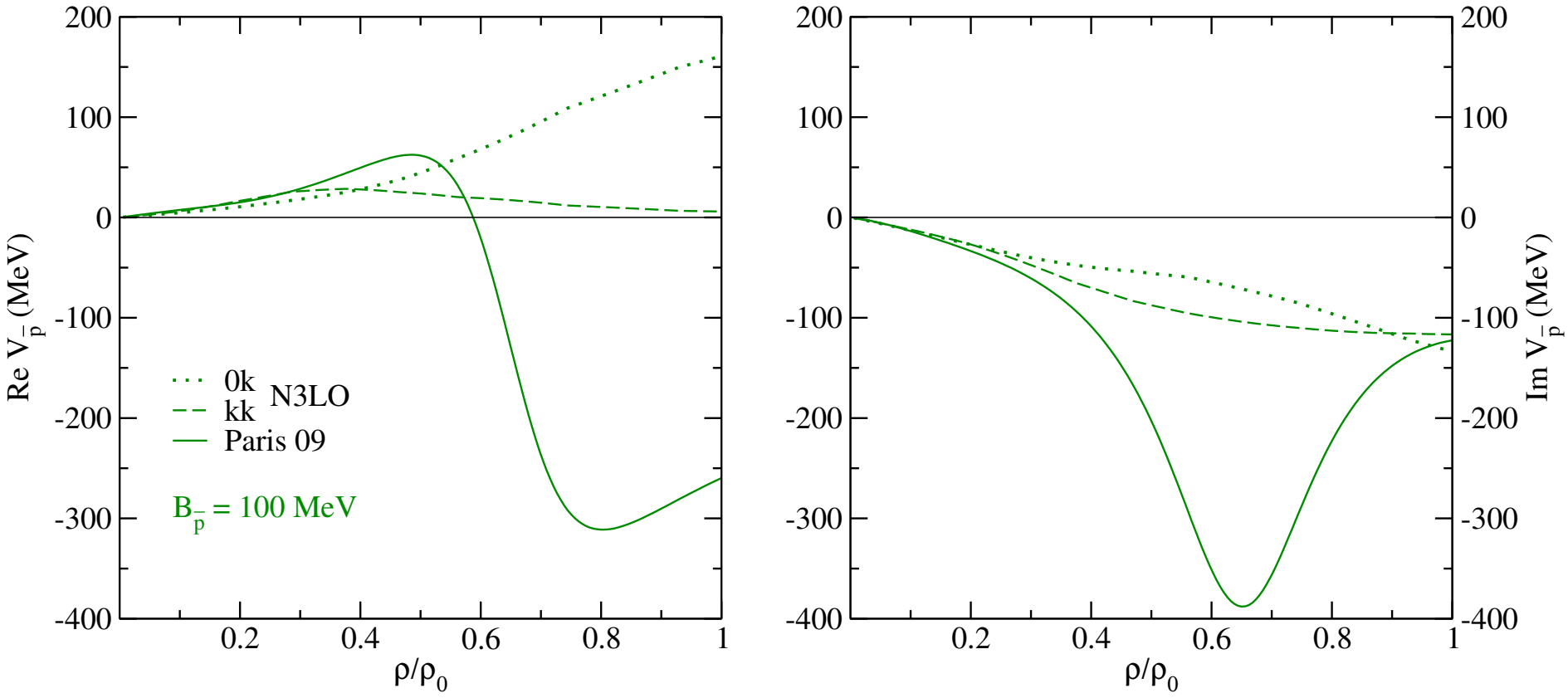

Fig.18: Real (left) and imaginary (right) $\bar{p}$ potentials in nuclear matter, calculated using the chiral N3LO and Paris 09 amplitudes for $B_{\bar{p}} = 100$ MeV.

N3LO vs. Paris 09 potential

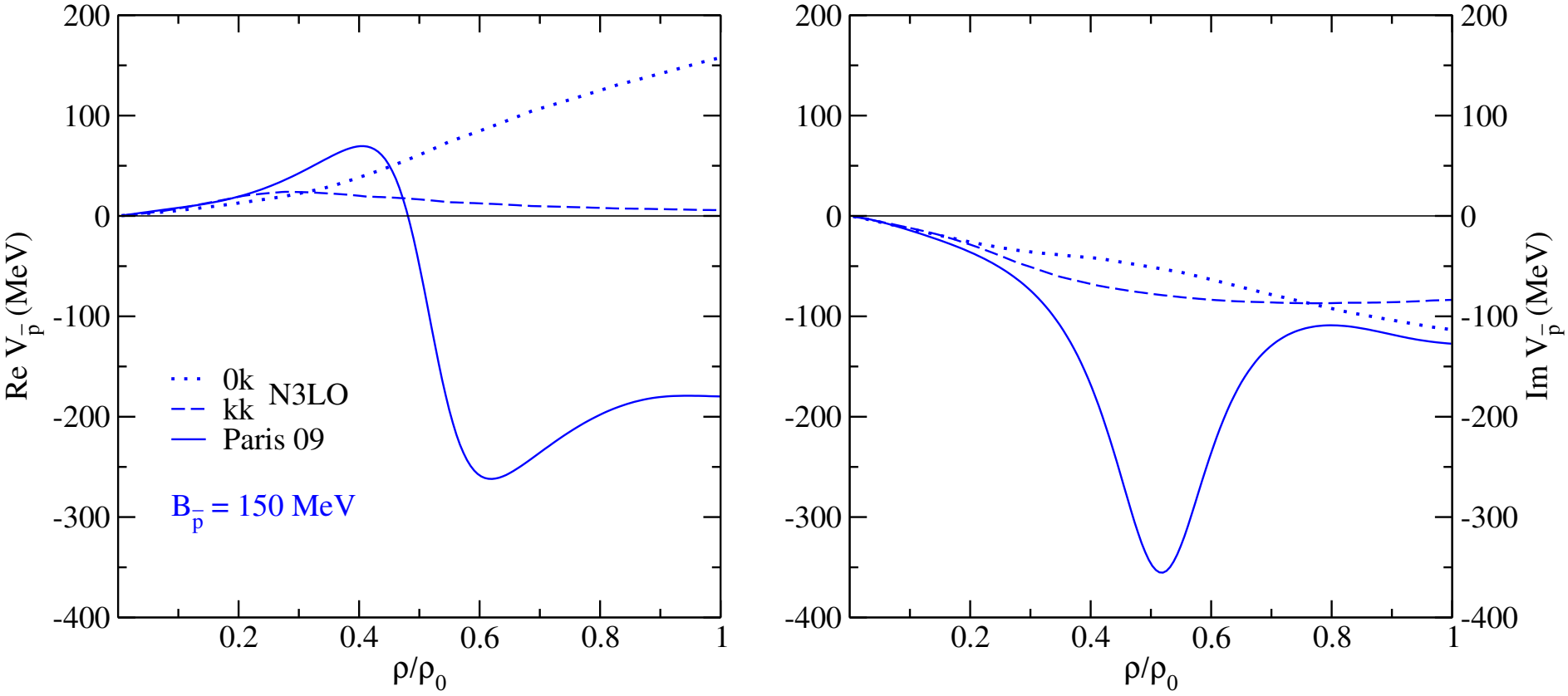

Fig.19: Real (left) and imaginary (right) $\bar{p}$ potentials in nuclear matter, calculated using the chiral N3LO and Paris 09 amplitudes for $B_{\bar{p}} = 150$ MeV.

Conclusions

- strong model dependence of the $\bar{N}N$ scattering amplitudes below threshold (Paris vs. N2LO vs. N3LO)
- $\bar{p}$ potential based on N2LO chiral amplitudes mildly attractive and absorptive below threshold
- $\bar{p}$ potential based on N3LO chiral amplitudes mildly attractive close to threshold threshold but further below threshold repulsive!
- more study needed

Thank you for your attention!